AIP | Applied Physics Letters

In-situ X-ray diffraction combined with scanning AC nanocalorimetry applied to a Fe0.84Ni0.16 thin-film sample

John M. Gregoire, Kechao Xiao, Patrick J. McCluskey, Darren Dale, Gayatri Cuddalorepatta et al.

Citation: Appl. Phys. Lett. **102**, 201902 (2013); doi: 10.1063/1.4806972
View online: http://dx.doi.org/10.1063/1.4806972
View Table of Contents: http://apl.aip.org/resource/1/APPLAB/v102/i20
Published by the AIP Publishing LLC.

In-situ X-ray diffraction combined with scanning AC nanocalorimetry applied to a $Fe_{0.84}Ni_{0.16}$ thin-film sample

John M. Gregoire,[1,a)] Kechao Xiao,[2] Patrick J. McCluskey,[3,a)] Darren Dale,[4] Gayatri Cuddalorepatta,[2] and Joost J. Vlassak[2,b)]
[1]*Joint Center for Artificial Photosynthesis, California Institute of Technology, 1200 E. California Blvd., Pasadena, California 91125, USA*
[2]*School of Engineering and Applied Sciences, Harvard University, 29 Oxford Street, Cambridge, Massachusetts 02138, USA*
[3]*GE Global Research, One Research Circle, Niskayuna, New York 12309, USA*
[4]*Cornell High Energy Synchrotron Source, Ithaca, New York 14853, USA*

(Received 4 April 2013; accepted 2 May 2013; published online 21 May 2013)

We combine the characterization techniques of scanning AC nanocalorimetry and x-ray diffraction to study phase transformations in complex materials system. Micromachined nanocalorimeters have excellent performance for high-temperature and high-scanning-rate calorimetry measurements. Time-resolved X-ray diffraction measurements during *in-situ* operation of these devices using synchrotron radiation provide unprecedented characterization of thermal and structural material properties. We apply this technique to a $Fe_{0.84}Ni_{0.16}$ thin-film sample that exhibits a martensitic transformation with over 350 K hysteresis, using an average heating rate of 85 K/s and cooling rate of 275 K/s. The apparatus includes an array of nanocalorimeters in an architecture designed for combinatorial studies. [http://dx.doi.org/10.1063/1.4806972]

Scanning calorimetry (SC) and x-ray scattering are powerful methods of materials characterization, the former quantifying thermal properties and the latter providing structural information. In a typical scanning calorimetry measurement, a phase transformation or solid-state reaction is efficiently explored through a temperature sweep, providing characterization of transformation or reaction temperature, latent heat, and the heat capacities of reactants and products.[1,2] As shown below, scanning calorimetry may require complementary methods to sufficiently characterize the material reaction. In the common case of crystalline phases, the complementary crystallographic characterization of powder x-ray diffraction (XRD) can provide the additional information required for a more complete understanding of the material reaction.

Experiments combining these two techniques have been performed at scanning rates less than 1 K/s,[3–8] limited by the scanning rate of bulk calorimeters and the data acquisition rate of traditional diffractometers. Nanocalorimetry has pushed accessible scanning rates to above 10^5 K/s.[9,10] This technique has enabled the study of materials far from equilibrium[11–15] and in particular has been combined with room-temperature diffraction measurements to elucidate the glass-forming behavior of metallic glasses.[16] Here, we demonstrate a combination of *in-situ* time-resolved XRD and nanocalorimetry measurements, and apply them to the study of a $Fe_{0.84}Ni_{0.16}$ thin-film sample.

The nanocalorimetry measurements in this study were performed using a parallel nano-SC (PnSC). The PnSC is a micromachined device described in detail elsewhere.[17–19] Briefly, it consists of a silicon substrate with a 5×5 array of independently controlled calorimeter sensors as shown in Fig. 1. Each sensor contains a tungsten four-point electrical probe that serves both as a heating element and a resistance thermometer and is fully encapsulated in a silicon nitride membrane. In a typical calorimetry measurement, a thin-film sample is deposited in the shaded area between the two sensing leads and an electric current is supplied through the tungsten heating element. The measured current and voltage are used to determine the power supplied to the sample, while the temperature of the sample is determined from the resistance of the heating element, which is calibrated to temperature.

For *in-situ* XRD characterization of an operating nanocalorimetry device, data acquisition rates providing a nominal temperature resolution of approximately 10 K or better is desirable. This rapid XRD acquisition rate is coupled with the additional challenge of weak diffraction intensity, due to the small ($\sim 10^2$ nm thick, 0.1–1 μg) samples typical of nanocalorimetry. To exploit the combinatorial capabilities of the PnSC device, the XRD measurement must be amenable to a broad range of materials and thus access a large region of reciprocal space. To meet these requirements, we developed a highly specialized pilot experiment at the Cornell High Energy Synchrotron Source (CHESS) A2 beam line. A lightly sanded Si-111 double-crystal monochromator provided a 30 keV x-ray beam with a flux of 4.5×10^{10} photons per second in the 0.6×1 mm beam cross-section. Following strategies outlined previously,[20] a large-area pixel array detector (GE 41RT) optimized for efficient detection of high-energy x rays was used in transmission geometry to acquire diffraction data (see Fig. 1). The detector can image as fast as 30 frames per second. For this experiment, a 0.2 s integration time was used during the nanocalorimetry measurement with additional 100 s integrations at room temperature, before and after the temperature scan. Diffraction images acquired from a blank membrane were used to subtract sources of scattering not

[a)]This research was performed while the authors were at the School of Engineering and Applied Sciences, Harvard University, 29 Oxford Street, Cambridge, Massachusetts 02138, USA.
[b)]E-mail: vlassak@esag.harvard.edu

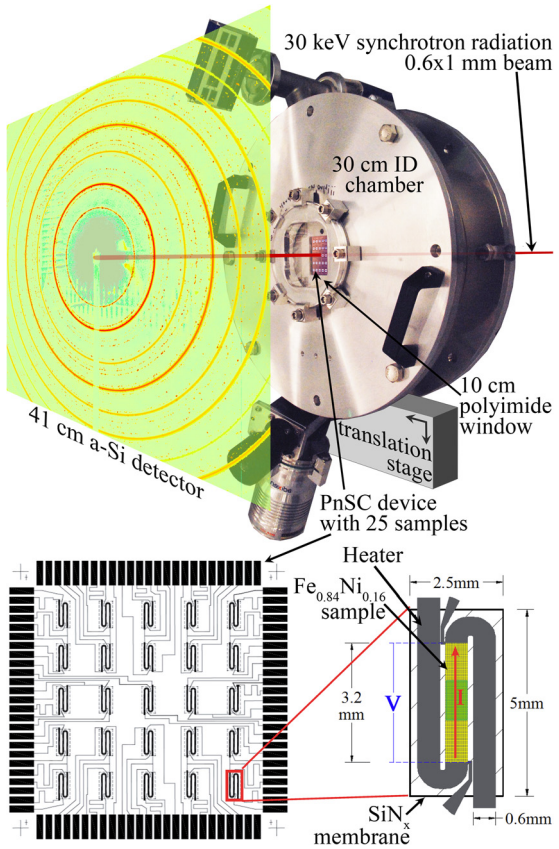

FIG. 1. (Top) Schematic of the combined nanocalorimetry and synchrotron XRD experiment showing the path of the 30 keV synchrotron beam through the vacuum chamber and nanocalorimeter device. The device can be seen through the polyimide window and the detector region is represented by a measured diffraction image. (Bottom) The metallization of the PnSC device is shown along with the detailed view of a single serpentine sensor that provides uniform sample heating over a broad range of scanning rates. The footprint of the x-ray beam is highlighted.

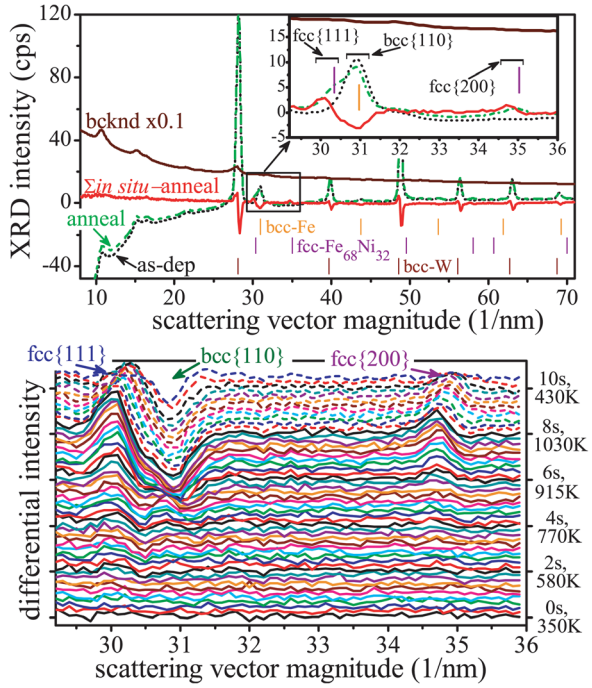

FIG. 2. Summary of XRD results. (Top) Powder patterns showing the XRD background as well as the XRD characterization of the as-deposited sample and annealed sample. The sum of the *in-situ* measurements (Σ *in-situ* anneal) is shown. Comparison with the peak positions of the noted phases shows the presence of fcc and bcc phases. (Bottom) The 54 powder patterns from the *in-situ* experiment after subtracting the initial room temperature pattern. The patterns are ordered as a function of time as noted on the right ordinate axis. Dashed patterns correspond to the cooling segment of the experiment. During the experiment, the sample was heated at an average rate of 85 K/s, followed by a quench at an average rate of 275 K/s.

associated with the sample of interest. The resulting diffraction images were then azimuthally integrated to provide 1-dimensional powder patterns (see Fig. 2).

To control the atmosphere during the calorimetry experiment, the measurements were performed inside a small custom-built vacuum chamber with internal diameter of 30 cm, which accommodated the PnSC device and probe card. To align the x-ray beam with each of the calorimeter samples in the 5×5 array, the chamber was mounted on a two-dimensional translation stage. The chamber contained an upstream x-ray window slightly larger than the PnSC device size and a considerably larger downstream window to avoid obstructing the diffraction cone from each calorimeter. The chamber was evacuated to a base pressure of 10^{-4} Pa, and measurements were performed in a controlled atmosphere of 20 Pa water vapor.

Nanocalorimetry measurements were performed using a data acquisition system controlled with Labview®, and were synchronized with the XRD acquisition systems via a TTL trigger. The data acquisition electronics were similar to those described in Refs. 17 and 20 with modifications for creating a compact, portable system. Computer control and measurements were performed through a digital-to-analog (DA) and analog-to-digital (AD) module (National Instruments NI cDAQ-9174 integrated with NI 9263 and NI 9205). The DA module was used to control a modified Howland current source, which powered the heating element in series with a precision resistor that was used for measuring the applied current. Noise reduction strategies included ground shielding, pseudo-differential sampling, optically isolated computer interfacing, and ground-isolated direct current (DC) power supplies (Agilent E3630A and E3620A).

A carefully designed current profile, containing DC and alternating current (AC) components, was applied to the PnSC device to attain the desired heating and cooling rates, and maximum temperature. The AC frequency $f = 416.67$ Hz produced temperature oscillations of approximately 6 K. As described in detail elsewhere,[17] the nonlinear thermal response of the PnSC device yielded harmonic injection into the measured sensor voltage. This sensor voltage was not only monitored for temperature determination through the calibrated resistance thermometer but also processed for harmonic analysis. By determining both the amplitude V_{2f} of the $2f$ harmonic and the phase angle of the temperature oscillation, φ_1, the heat capacity of the sample and addendum was calculated as[17,20]

$$mC_p = \frac{i^2 I_0 R_0 k}{2\pi f |V_{2f}|} \sqrt{\frac{25\tan^2\varphi_1 + 9}{16\tan^2\varphi_1 + 4} \times \frac{\tan^2\varphi_1}{1 + \tan^2\varphi_1}}, \quad (1)$$

where I is the DC component of the applied current, i is the AC amplitude, R_0 is the resistance of the calorimetry sensor, and k is its temperature derivative. This expression is the result of a recently developed scanning AC nanocalorimetry

technique,[17,20] which has broadened the usable scanning rate and enabled *in-situ* experiments such as that described here. The measured sensor voltage was partitioned into segments containing two cycles and Eq. (1) was evaluated for each segment to provide mC_p as a function of time and temperature, which comprises the calorimetric measurement of the sample.

After fabrication of the PnSC device, the sensor was calibrated to determine the R_0 and k values using established techniques.[17,18] A 180 nm film of $Fe_{0.84}Ni_{0.16}$ was deposited using magnetron co-sputtering from elemental sources in a DC magnetron deposition system (AJA International) with base pressure of 1×10^{-5} Pa. The Fe and Ni sources (2 in. diameter) were powered at 120 W and 18 W, respectively, and the 37-min deposition proceeded in an atmosphere of 0.67 Pa of Ar. A test sample deposited under identical conditions was analyzed with Energy Dispersive Spectroscopy and profilometry to determine film composition and thickness. The deposition was performed through a shadow mask onto the PnSC sensor region to provide a calorimetry sample of approximately 50 nmol.

In the as-deposited state, the primary phase of the Fe-Ni film is bcc, as indicated in Fig. 2 by the match to the bcc-Fe pattern (4-014-0360, Ref. 21). Before the *in-situ* experiment, the sample was twice heated to 1100 K in vacuum and cooled to room temperature at rates of approximately 2×10^4 K/s. This annealing procedure ensured that the sample was highly crystalline, and resulted in the formation of a second phase, fcc-(Fe,Ni) with a mole fraction of approximately 30% (see Fig. 2 with fcc-$Fe_{68}Ni_{32}$ pattern 04-002-1863, Ref. 21). The grain size in the sample after the annealing step was estimated to be at least 30 nm based on a Scherrer analysis of the diffraction peak widths. According to the Fe-Ni phase diagram,[22] the fcc phase is stable at elevated temperature, while the room-temperature equilibrium phase structure of the sample is a mixture 80% bcc-(Fe,Ni) and 20% of the ordered $FeNi_3$ intermetallic compound. However, formation of the compound requires considerable diffusion and is not favored under the rapid-cooling conditions of this experiment—the diffusion distance of Ni in Fe on the timescale of the experiment is less than 1 nm.[23] This notion, along with the larger fraction of fcc phase in our measurements, suggests that upon cooling the high-temperature fcc phase undergoes a martensitic transformation to form a supersaturated bcc phase.[22]

The fcc + bcc phase mixture noted above was the starting state of the *in-situ* experiment, during which the sample was heated at an average rate of 85 K/s and then quenched at an average rate of 275 K/s. To illustrate the evolution of the XRD patterns during the *in-situ* experiment, Fig. 2 shows the XRD difference spectra with respect to the initial pattern. The behavior of the fcc {111}, bcc {110}, and fcc {200} peaks is readily ascertained from the series of differential diffraction patterns. The quantitative analysis of the peak intensities is shown in Fig. 3, where the peak intensities for each phase have been normalized by the intensities obtained during the 100 s ambient temperature measurements. Because the martensitic transformation is diffusionless, both phases have the same composition and the structure factors can be calculated. Given the fcc {111} and bcc {110} peak intensities, the mole fractions of the two phases can be plotted as a function of temperature/time, as seen in Fig. 3.

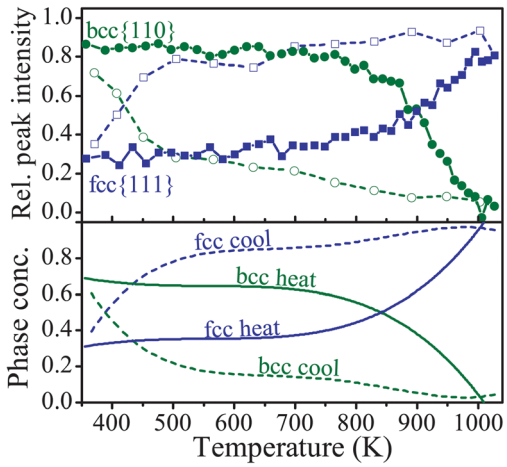

FIG. 3. (Top) Quantitative results of Fig. 2 showing the temperature evolution of the bcc and fcc peaks during the heating (solid lines) and cooling (dashed lines) segments of the *in-situ* experiment. Peak intensities are relative to the room temperature values prior to the *in-situ* experiment. (Bottom) Phase concentrations derived from the above data. Concentrations have been smoothed using fifth-order polynomial fitting. During the experiment, the sample was heated at an average rate of 85 K/s, followed by a quench at an average rate of 275 K/s.

During the 800-1020 K portion of the heating segment, the bcc phase transforms into the fcc phase. Upon quenching, the sample remains at least 80% in the fcc phase until 500 K and approaches its original phase composition by 360 K. The temperature hysteresis associated with this martensitic transformation is in excess of 350 K and is directly observed by the high-speed XRD measurement. The presence of the fcc phase at room temperature indicates that the martensitic transformation is not complete and has shifted to lower temperatures than reported measurements for bulk samples.[24] This shift is commonly observed for martensitic transformations in materials with very fine microstructures.[18]

The heat capacity from the PnSC measurement is shown along with the scanning rate in Fig. 4. During the heating segment, mC_p varies smoothly until near 800 K, where an upward trend is observed. This upward trend is not sustained and is in fact reversed above 900 K, after which the mC_p signal decreases for the remainder of the heating and the entire cooling segment. Given the water vapor atmosphere, incorporation of oxygen into the sample via thermal oxidation could be suspected for the increased heat capacity at elevated temperature. This explanation is, however, not supported by the reversal in the mC_p trend or the return to its initial value at the end of the experiment, as any oxidation of the sample would be irreversible at these temperatures.

The behavior of the mC_p data can be understood by combining the XRD and PnSC results. The measured mC_p signal contains contributions from both fcc and bcc phases, as well as the calorimeter addenda (measured on a separate device). To resolve the heat capacity signals from the fcc and bcc phases, the C_p of the fcc phase was taken from the literature. Chen and Sundman[25] reported detailed calculation of the heat capacity of fcc-Fe, which is a slowly varying function of temperature over the range of our measurement. The average value of C_p in this temperature range is approximately 31 J/K/mol, but we found that meaningful interpretation of the measured heat capacity for $Fe_{0.84}Ni_{0.16}$ was

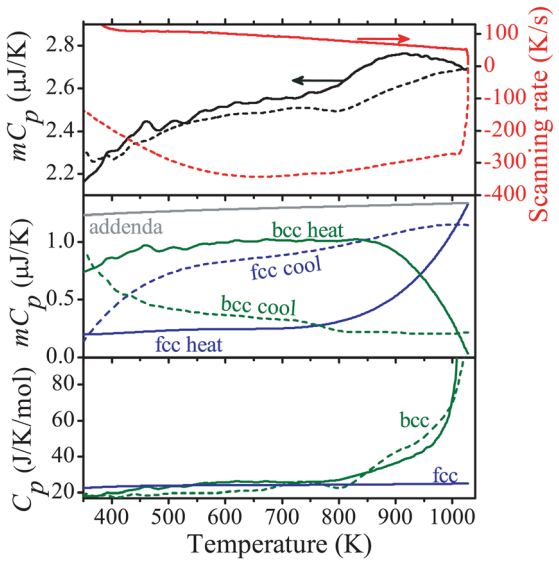

FIG. 4. (Top) The PnSC results showing the measured heat capacity during the heating (solid lines) and cooling (dashed lines) segments of the *in situ* experiment along with the scanning rate. (Middle) Deconvolution of the measured heat capacity into addenda, fcc, and bcc components. The sum of these components equals the measured heat capacity at each temperature. (Bottom) The assumed fcc and ascertained bcc specific heat capacities.

attained by scaling the literature value by 0.76. The heat capacity of the nanoscale sample may be smaller than the bulk literature value, or this required scaling may be due to overestimation of the sample size or addenda heat capacity.

The mC_p signal of the fcc phase was modeled by multiplying the scaled C_p for fcc-Fe by both the sample size of 50 nmol and the phase concentration from Fig. 3. This permitted calculation of the bcc contribution to the measured mC_p and thus the specific heat capacity of bcc-$Fe_{0.84}Ni_{0.16}$ (see Fig. 4). Ideally, the calculated C_p would be identical for the heating and cooling segments, and Fig. 4 shows that these two segments have the same trend with respect to temperature, with differences that are well within the experimental error and uncertainty of the above approximations. The result shows that below 750 K the heat capacity of the bcc phase is comparable to that of the fcc phase, but it increases at higher temperature and dramatically so near 1000 K, in agreement with bulk bcc-Fe.[25] The measured heat capacity indicates that the martensite is ferromagnetic with a Curie temperature near 1000 K, in good agreement with the established 1010 K Curie temperature for bcc-$Fe_{0.84}Ni_{0.16}$.[26]

By combining the XRD and PnSC measurements, detailed information was obtained on the transformation behavior of $Fe_{0.84}Ni_{0.16}$ at ultra-fast heating and cooling rates. Looking forward, we anticipate that this technique can also be used to study solid-gas reactions. For instance, elucidation of the oxidation kinetics of the $Fe_{0.84}Ni_{0.16}$ alloy could be performed by employing slower scan rates or isothermal measurements at elevated temperature. Such studies would be quite powerful for development of high-temperature oxidation resistant materials[27] or materials for thermochemical generation of fuel via water splitting.[28,29] The range of scattering vector magnitude measured in this experiment (see Fig. 2) is sufficient for structural characterization of solid-state materials. In general, the development of this combined calorimetry and diffraction experiment at unprecedented scanning rates creates the possibility for a broad range of new materials explorations, from reaction kinetics to the high-throughput mapping of phase transformations.

The authors thank Aaron Lyndaker for assistance with the synchrotron experiments and James MacArthur for assistance with the custom electronics. This work was supported by the Materials Research Science and Engineering Center at Harvard University (NSF-DMR-0820484), the Air Force Office of Scientific Research (FA9550-12-1-0098), and the DOE Office of Basics Energy Sciences (DE-SC-0004889). The experiments were conducted at CHESS, which is supported by the NSF & NIH/NIGMS via NSF Award No. DMR-0936384. Device fabrication was supported by the Center for Nanoscale Systems at Harvard University (NSF-ECS-0335765).

[1]F. Spaepen and C. V. Thompson, Appl. Surf. Sci. **38**(1–4), 1–12 (1989).
[2]C. Michaelsen, K. Barmak, and T. Weihs, J. Phys. D: Appl. Phys. **30**(23), 3167 (1997).
[3]Z. W. Yu and Y. Liu, J. Therm. Anal. Calorim. **58**(2), 363–368 (1999).
[4]T. Arii, A. Kishi, and Y. Kobayashi, Thermochim. Acta **325**(2), 151–156 (1999).
[5]A. Kishi and H. Toraya, Powder Diffr. **19**(1), 31–35 (2004).
[6]A. Yebra-Rodriguez, P. Alvarez-Lloret, A. B. Rodriguez-Navarro, J. D. Martin-Ramos, and C. Cardell, Mater. Lett. **63**(13–14), 1159–1161 (2009).
[7]A. Kishi, M. Otsuka, and Y. Matsuda, Colloid Surf., B **25**(4), 281–291 (2002).
[8]H. Yoshida, R. Kinoshita, and Y. Teramoto, Thermochim. Acta **264**, 173–183 (1995).
[9]M. Y. Efremov, J. Warren, E. Olson, M. Zhang, A. Kwan, and L. Allen, Macromolecules **35**(5), 1481–1483 (2002).
[10]M. Y. Efremov, E. A. Olson, M. Zhang, F. Schiettekatte, Z. Zhang, and L. H. Allen, Rev. Sci. Instrum. **75**(1), 179–191 (2004).
[11]S. Lai, G. Ramanath, L. Allen, P. Infante, and Z. Ma, Appl. Phys. Lett. **67**, 1229 (1995).
[12]T. F. J. Pijpers, V. B. F. Mathot, B. Goderis, R. L. Scherrenberg, and E. W. van der Vegte, Macromolecules **35**(9), 3601–3613 (2002).
[13]E. A. Olson, M. Y. Efremov, M. Zhang, Z. Zhang, and L. H. Allen, J. Microelectromech. Syst. **12**(3), 355–364 (2003).
[14]A. Minakov, S. Adamovsky, and C. Schick, Thermochim. Acta **432**(2), 177–185 (2005).
[15]B. Revaz, B. Zink, and F. Hellman, Thermochim. Acta **432**(2), 158–168 (2005).
[16]J. M. Gregoire, P. J. McCluskey, D. Dale, S. Ding, J. Schroers, and J. J. Vlassak, Scr. Mater. **66**(3), 178–181 (2012).
[17]K. Xiao, J. M. Gregoire, P. J. McCluskey, and J. J. Vlassak, Rev. Sci. Instrum. **83**(11), 114901–114915 (2012).
[18]P. J. McCluskey and J. J. Vlassak, J. Mater. Res. **25**(11), 2086–2100 (2010).
[19]P. J. McCluskey and J. J. Vlassak, Thin Solid Films **518**(23), 7093–7106 (2010).
[20]J. M. Gregoire, K. Xiao, P. J. McCluskey, D. Dale, and J. J. Vlassak, "Scanning AC nanocalorimetry combined with in-situ X-Ray Diffraction," J. Appl. Phys. (submitted).
[21]Powder Diffraction File, "PDF-2, release 2004," The International Centre for Diffraction Data (ICDD), 12, 2005.
[22]L. Swartzendruber, V. Itkin, and C. Alcock, J. Phase Equilib. **12**(3), 288–312 (1991).
[23]M. L. Yunker and J. A. Van Orman, Earth Planet. Sci. Lett. **254**(1), 203–213 (2007).
[24]L. Kaufman and M. Cohen, Trans. AIME **206**, 1393 (1956).
[25]Q. Chen and B. Sundman, J. Phase Equilib. **22**(6), 631–644 (2001).
[26]M. Peschard, *Thèses présentées à la Faculté des sciences de l'Université de Strasbourg. par M. Marcel Peschard, Contribution à l'étude des ferro-nickels* (éditions de la "Revue de métallurgie, 1925).
[27]D. R. Clarke and S. R. Phillpot, Mater. Today **8**(6), 22–29 (2005).
[28]M. D. Allendorf, R. B. Diver, N. P. Siegel, and J. E. Miller, Energy Fuels **22**(6), 4115–4124 (2008).
[29]J. R. Scheffe, M. D. Allendorf, E. N. Coker, B. W. Jacobs, A. H. McDaniel, and A. W. Weimer, Chem. Mater. **23**(8), 2030–2038 (2011).